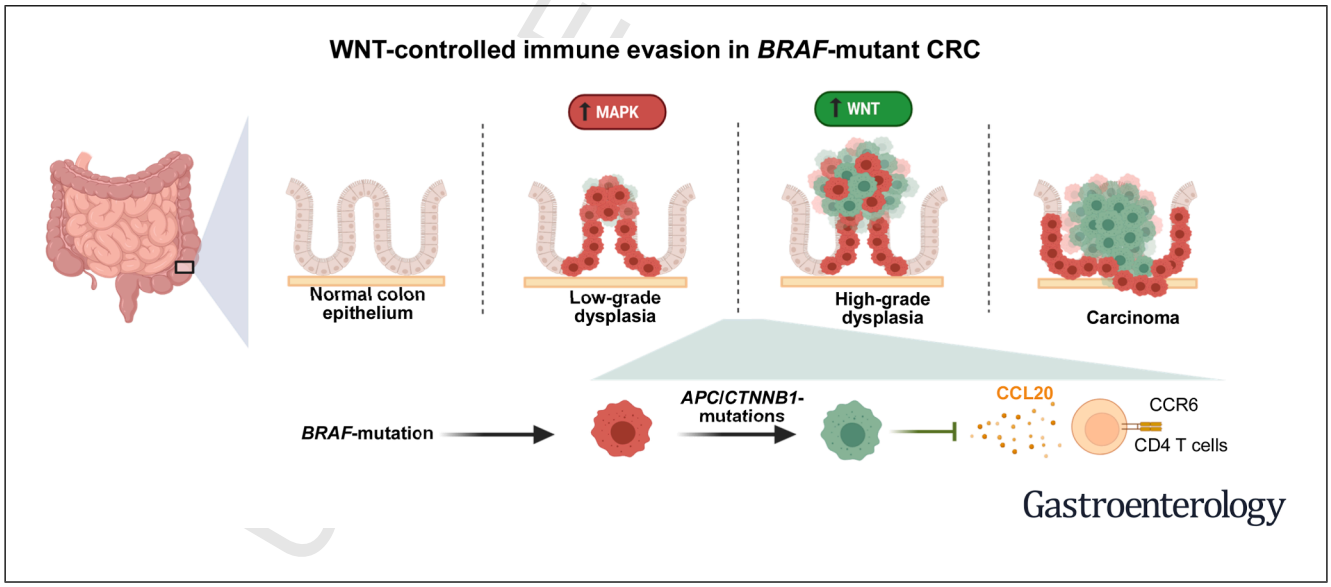
Gastroenterology 2026;■:1–15

WNT-Driven Immune Evasion Promotes Malignant Transformation of *BRAF*-Mutant Colorectal Cancer

Manuel Mastel,[1,2] Aitana Guiseris Martinez,[1,2,3] Umberto Pozza,[1,2] Jasmin Meier,[1,2] Ioannis Chiotakakos,[1,2,3] Sandra Jaun,[1,2] Carolin Artmann,[1,2] Gabriele Diamante,[1,2,3] Nikolaos Georgakopoulos,[1,2,3] Philipp Albrecht,[3,4] Yvonne Petersen,[4] Saskia Reuter,[5,6] Barbara Schmitt,[5,6] Michael Günther,[7] Alexandra Thiran,[1,2] Istiffa Nurfauziah,[1,8] Ian Ghezzi,[1,8] Kyanna S. Ouyang,[3,9,10] Michael D. Milsom,[1,8] Jens Puschhof,[3,9,10,11] Nic G. Reitsam,[12,13,14] Kim E. Boonekamp,[5,6] Johannes Betge,[4,11,15,16,17] Steffen Ormanns,[7] Michael Boutros,[5,6,11] and Rene Jackstadt[1,2,11]

[1]Heidelberg Institute for Stem Cell Technology and Experimental Medicine (HI-STEM gGmbH), Heidelberg, Germany; [2]Cancer Progression and Metastasis Group, German Cancer Research Center (DKFZ) and DKFZ-ZMBH Alliance, Heidelberg, Germany; [3]Faculty of Biosciences, Heidelberg University, Heidelberg, Germany; [4]Junior Clinical Cooperation Unit Translational Gastrointestinal Oncology and Preclinical Models, German Cancer Research Center (DKFZ), Heidelberg, Germany; [5]Division of Signaling and Functional Genomics, German Cancer Research Center (DKFZ), Heidelberg, Germany; [6]Heidelberg University, Institute for Human Genetics, Department of Molecular Human Genetics & BioQuant, Medical Faculty, Heidelberg, Germany; [7]Institute of General Pathology, Medical University Innsbruck, Austria; [8]Division of Experimental Hematology, German Cancer Research Center (DKFZ), and DKFZ-ZMBH Alliance, Heidelberg, Germany; [9]Epithelium Microbiome Interaction Laboratory, German Cancer Research Center (DKFZ), Heidelberg, Germany; [10]DKFZ Hector Cancer Institute, University Medicine Mannheim, Heidelberg, Germany; [11]German Cancer Consortium (DKTK), German Cancer Research Centre (DKFZ), Heidelberg, Germany; [12]Bavarian Cancer Research Center (BZKF) and KIONET, Augsburg, Germany; [13]Pathology, Faculty of Medicine, University of Augsburg, Augsburg, Germany; [14]Else Kroener Fresenius Center for Digital Health, Technical University Dresden, Dresden, Germany; [15]Department of Medicine II, University Medical Center Mannheim, Medical Faculty Mannheim, Heidelberg University, Mannheim, Germany; [16]DKFZ Hector Cancer Institute at University Medical Center Mannheim, Mannheim, Germany; and [17]Mannheim Cancer Center, Medical Faculty Mannheim, Heidelberg University, Mannheim, Germany



BACKGROUND & AIMS: *BRAF*-mutant colorectal cancer (CRC) is a clinically aggressive subtype arising from the serrated pathway and is associated with poor prognosis and therapy resistance. The mechanisms driving malignant transformation in microsatellite-stable (MSS) *BRAF*-mutant CRC remain incompletely understood. We aimed to define the role of WNT pathway activation in serrated CRC progression and tumor-immune interactions. **METHODS:** We generated multiple genetically engineered mouse models of *BRAF*-mutant MSS CRC and complementary organoid-based transplantation models. Genetic alterations in WNT pathway components were functionally interrogated. Tumor development and immune microenvironment remodeling were analyzed using bulk RNA sequencing, single-cell RNA sequencing, Cellular Indexing of

Transcriptomes and Epitopes by Sequencing, and functional in vivo assays. **RESULTS:** WNT pathway activation via *APC* or *CTNNB1* mutations, but not *RNF43* loss, was required for tumor initiation in *BRAF*-mutant CRC models. WNT activation induced a molecular subtype shift and suppressed immune response pathways. Mechanistically, WNT signaling suppressed C-C motif chemokine ligand 20 expression and remodeled the tumor microenvironment by promoting immunosuppressive myeloid populations and altering T-cell states. Functional assays demonstrated that WNT activation enhances tumor progression in immunocompetent settings, indicating immune evasion as a key driver of malignant progression. **CONCLUSIONS:** WNT pathway activation is a critical determinant of malignant transformation in *BRAF*-mutant MSS CRC by enabling immune escape. These findings identify WNT signaling as a central regulator of tumor-immune interactions and a potential therapeutic target in this aggressive CRC subtype.

Keywords: Serrated Neoplasia; WNT Signaling; Tumor Microenvironment; Mouse Models.

WHAT YOU NEED TO KNOW

BACKGROUND AND CONTEXT

BRAF-mutant colorectal cancer develops through the serrated pathway and is associated with poor prognosis and limited treatment options. The mechanisms driving malignant transformation, particularly in microsatellite-stable tumors, remain poorly understood.

NEW FINDINGS

Using genetically engineered mouse models and organoid systems, we show that activation of WNT signaling through *APC* or *CTNNB1* mutations is required for tumor initiation. WNT activation promotes immune evasion by reshaping the tumor microenvironment and impairing T-cell function, enabling tumor progression and metastasis.

LIMITATIONS

Findings are primarily based on mouse models and organoid systems, which may not fully capture human tumor complexity. Further validation and clinical studies are required.

CLINICAL RESEARCH RELEVANCE

The results suggest new opportunities for combination therapies targeting WNT signaling and antitumor immunity in *BRAF*-mutated colorectal cancer.

BASIC RESEARCH RELEVANCE

The results identify WNT signaling as a key driver of immune escape in *BRAF*-mutant colorectal cancer.

Colorectal cancer (CRC) can arise through distinct molecular and histopathological routes.[1–3] In addition to the classical pathway, CRC can develop via a more aggressive serrated route, characterized by precursor lesions with saw-tooth–like histology.[1] The serrated pathway accounts for ∼20% of CRC, is enriched in the right colon, and often produces flat lesions that are difficult to detect by colonoscopy, thus representing a clear unmet clinical need.[4] Morphologically, serrated precursor lesions can be classified as hyperplastic polyps, sessile serrated adenomas (SSAs)/polyps, and traditional serrated adenomas.[5] Initiation events of serrated lesions are activating point mutations in *BRAF* or *KRAS,* leading to enhanced MAPK signaling and increased proliferation.[6,7] $BRAF^{V600E}$ hotspot mutations are found in ∼10% of CRCs and are associated with SSA precursors and define a clinically distinct subgroup characterized by poor prognosis and low response rates to conventional chemotherapies.[8,9] *BRAF*-activated serrated human tumors exhibit characteristic DNA methylation patterns (CpG island methylator phenotype) and nuclear β-catenin localization, indicative of tumor-associated activation of the WNT/β-catenin pathway.[10,11] Approximately half of serrated CRCs are microsatellite instability (MSI), often through *MLH1* silencing and respond well to immune checkpoint inhibition (ICI).[12] The remainder are microsatellite stable (MSS), although *BRAF*-mutant MSS tumors comprise only 3.4% to 7.1% of CRC, they follow a particularly aggressive clinical course.[13–15]

Although estimations predict that 20% to 30% of CRC arises from serrated precursor lesions, only ∼10% of CRCs actually present with serrated features.[16] For better functional understanding of disease progression, genetically engineered mouse models (GEMMs) serve as useful and important tools.[17] Mice harboring oncogenic *BRAF* develop widespread serrated hyperplasia that progresses with age to dysplastic serrated adenomas but rarely to metastatic carcinoma. These advanced lesions exhibit enhanced MAPK activity and activating WNT/β-catenin mutations.[6,18] Immunohistochemical analyses of human SSAs show that nuclear β-catenin is found in serrated lesions with neoplastic potential.[10] However, some *BRAF*-mutant mouse models develop tumors without detectable WNT activation, indicating heterogeneity in pathway dependence.[1]

Cancer cells influence their surroundings by secreting cytokines, chemokines, and growth factors that reprogram immune and stromal cells to adopt pro-tumorigenic phenotypes.[19] The composition of factors that are produced by cancer cells may be instructed by cell-intrinsic cues such as their genetics or epigenetics.[20,21] Particularly, T cells are central to adaptive antitumor immunity, capable of directly recognizing and killing malignant cells.[19] Therapeutic strategies targeting *BRAF*-mutant CRC by inhibiting the

Abbreviations used in this paper: **4-OHT, 4-Hydroxytamoxifen; CCL20, C-C motif chemokine ligand 20; CCR6, C-C chemokine receptor type 6; CITE-seq, Cellular Indexing of Transcriptomes and Epitopes by Sequencing; CMS, consensus molecular subtype; CRC, colorectal cancer; EGFR, epidermal growth factor receptor; GEMM, genetically engineered mouse model; ICI, immune checkpoint inhibition; IFN, interferon; MSI, microsatellite instability; MSS, microsatellite stable; PBS, phosphate-buffered saline; SSA, sessile serrated adenoma.**

© 2026 The Author(s). Published by Elsevier Inc. on behalf of American Gastroenterological Association Institute. This is an open access article under the CC BY license (http://creativecommons.org/licenses/by/4.0/).
0016-5085
https://doi.org/10.1053/j.gastro.2026.07.035

UNCORRECTED

MAPK pathway have been proven challenging due to rapid feedback activation and pathway redundancy.[22] Combination strategies, such as BRAF inhibition combined with MEK or epidermal growth factor receptor (EGFR) inhibition, have shown promise in improving outcomes for patients with *BRAF*-mutant CRC.[23] Interestingly, alterations in *RNF43*, a negative regulator of WNT signaling, showed predictive capacity for response to BRAF/EGFR inhibition.[24] Resistance to BRAF/EGFR was found to be driven by ERK-independent, SRC -mediated transcriptional reprogramming via β-catenin signaling.[25] Again, this indicates a central role for WNT signaling in therapy resistance of *BRAF*-mutant CRC. Recently, therapeutic efficacy has been successfully extended by combining ICI with BRAF/MEK or BRAF/EGFR targeting.[26,27] This highlights the potential for combinatorial therapies, including ICIs, and underscores the importance of understanding the tumor immune microenvironment in *BRAF*-mutant CRC.

Limited understanding of the transition from SSA to serrated CRC emphasizes the need for improved mechanistic insight into pathways and processes driving this malignant transformation. Here we generated multiple GEMMs and used organoid transplantation models to dissect genetic events driving the progression of *BRAF*-mutant CRC. Because the role of WNT signaling in serrated CRC is poorly defined, we examined recurrent WNT pathway alterations identified in our GEMMs and patient cohorts. We found that WNT pathway activation through *APC* or *CTNNB1* mutations was required for SSA transformation. Mechanistic characterization showed that WNT activation drives immune evasion in serrated CRC by impairing T-cell phenotypes. Ultimately, this opens opportunities to test novel immunotherapy strategies for WNT-altered MSS CRC.

Materials and Methods

Details on overexpressing vectors, virus production, ethical statement for human samples, mismatch repair/MSI analysis of human samples, *BRAF* mutational analysis of human samples, pathological evaluation of lesion progression, animal experiments, in vitro organoid growth, genome editing validation, flow cytometry, immunofluorescence, immunohistochemistry, in situ hybridization, tumor dissociation, quantitative polymerase chain reaction, single-cell sequencing data generation and analysis, Cellular Indexing of Transcriptomes and Epitopes by Sequencing (CITE-seq) data generation and analysis, RNA sequencing, tumor bulk consensus molecular subtype (CMS) classification, human single-cell sequencing data set analysis, survival analysis by CMS, whole-exome sequencing, mutational profiling of *BRAF*-mutant CRC from publicly available data, drug screening of murine cancer organoids, and analysis of drug sensitivities are available in the Supplementary Materials.

CRISPR Knockout and Base Editing Vectors

CRISPR genomic engineering vectors were generated via conventional oligo cloning strategies. Plasmids are shown in Supplementary Table 1. Base editing contains a dCas9 domain coupled to a cytosine deaminase (APOBEC). This facilitates the deamination of a cytosine (C), leading to an uracil base (U), which is then read as thymine (T). F2X is a base editor previously designed.[28]

Colonoscopy-Guided Submucosal Injection

Intracolonic injection was performed with 4-Hydroxytamoxifen (4-OHT) for VBPN, VBPNA, VBPNC, and VBPNR mouse models. Colonoscopic delivery of 4-OHT was performed following established protocols.[29] Briefly, mice were anesthetized using isoflurane, and a portable veterinary endoscopy system (Karl Storz, Tele Pack Vet X LED) equipped with a Hopkins telescope (#67030 BA) was used. Injections were administered using a Hamilton syringe (#7656–01), a transfer needle (#7770–02), and a fine injection needle (#7803–05). Three separate injections of 70 μL each were delivered into the colon wall to create visible blebs. Tumor initiation and progression were monitored longitudinally via colonoscopy.

Generation of Mouse Organoids

Mouse colon organoids were generated following previously published protocols.[29] Briefly, colon tissue was excised, cut into ~5-mm fragments, and washed repeatedly in cold phosphate-buffered saline (PBS). After allowing tissue pieces to settle, the supernatant was removed, and the washing step was repeated until the supernatant appeared clear. The fragments were then incubated in PBS containing 25 mM EDTA for colon (Invitrogen, #AM9260G) for 30 minutes on a rotating platform at 4°C. Supernatant fractions were collected and examined, and the cleanest crypt-containing fraction was selected. These were pooled, passed through a cell strainer, and centrifuged to collect the crypts.

The resulting pellet was resuspended in Cultrex BME, reduced growth factor matrix (R&D Systems, #3433–005–01). Colon organoids were cultured in Advanced Dulbecco's modified Eagle's medium/F12 (Gibco, #12634028) supplemented with 1% L-Glutamine (Thermo Fisher Scientific, #25030024), 1% HEPES (Sigma, #H0887–100), 1% penicillin-streptomycin (Sigma, #P4458–100ML), 50% WRN-conditioned medium, 20% fetal bovine serum (Thermo Fisher Scientific, #A5256701), 50 ng/mL epidermal growth factor (Peprotech, #AF-100–15), 10 μM Y-27632 (Hölzel, #M1817), 0.5 μM A83–01 (Sigma, #SML0788), and 2 μL/mL Primocin (InvivoGen, #ant-pm-2).

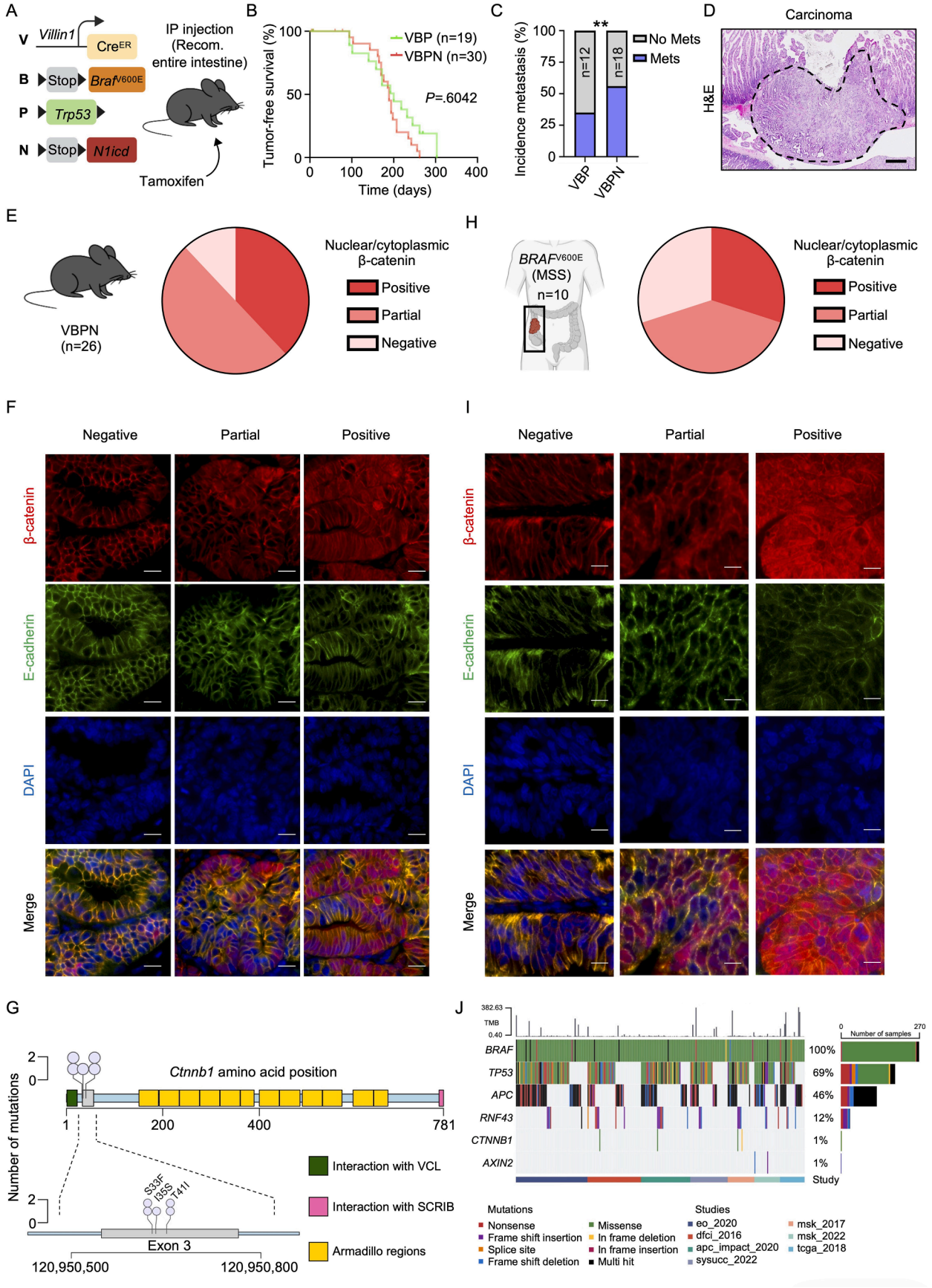
Organoid Genome Editing

DNA of organoid cultures was edited via CRISPR genetic engineering for the generation of specific knockouts and base edits. Organoids were cultured to confluency and subjected to plasmid electroporation. The mix was electroporated with NEPA21 electroporator (Nepagene). Electroporation was conducted with poring pulse: 175 V, 5-ms length, 50-ms interval, 2 intervals, 10% decay rate, and positive polarity and transfer pulse: 20 V, 50-ms length, 50-ms interval, 5 intervals, 40% decay rate, and ± polarity.

Organoid Transduction and Selection

Organoids were dissociated with TrypLE (Gibco, #12605010) and resuspended in 100 μL of complete media

UNCORRECTED PROOF


A
V Villin1 CreER
B Stop Braf V600E
P Trp53
N Stop N1icd
IP injection (Recom. entire intestine)
Tamoxifen
B
Tumor-free survival (%)
VBP (n=19)
VBPN (n=30)
P=.6042
Time (days)
C
Incidence metastasis (%)
**
n=12
n=18
No Mets
Mets
VBP
VBPN
D
Carcinoma
H&E
E
VBPN (n=26)
Nuclear/cytoplasmic β-catenin
Positive
Partial
Negative
H
BRAF V600E (MSS) n=10
Nuclear/cytoplasmic β-catenin
Positive
Partial
Negative
F
Negative
Partial
Positive
β-catenin
E-cadherin
DAPI
Merge
I
Negative
Partial
Positive
β-catenin
E-cadherin
DAPI
Merge
G
Number of mutations
Ctnnb1 amino acid position
Interaction with VCL
Interaction with SCRIB
Armadillo regions
S33F
I35S
T41I
Exon 3
120,950,500
120,950,800
J
TMB
Number of samples
BRAF 100%
TP53 69%
APC 46%
RNF43 12%
CTNNB1 1%
AXIN2 1%
Study
Mutations
Nonsense
Frame shift insertion
Splice site
Frame shift deletion
Missense
In frame deletion
In frame insertion
Multi hit
Studies
eo_2020
dfci_2016
apc_impact_2020
sysucc_2022
msk_2017
msk_2022
tcga_2018

with 10 μg/mL of Polybrene (Sigma, #TR-1003); 100 μL of the lentiviral particles containing the Ccl20-expressing plasmid and the respective empty vector were added to the organoid suspension and the mix was spun down at 32°C for 30 minutes and incubated at 37°C for 1 hour. Transduced organoids were plated in 70% BME. Four to 5 days after transduction, organoids were selected via antibiotic selection.

Organoid Treatments

To modulate Wnt pathway activity in vitro, cells were treated with WNT Surrogate-Fc Fusion Protein (Wnt-Fc, AVS bio, #IPA-N001) at 200 ng/mL or with a Glycogen Synthase Kinase-3 inhibitor (CHIR-99021, Sigma-Aldrich, #SML1046) at 3 μM. Treatments were maintained for 24 and 48 hours, respectively.

Subcutaneous Injection, Tumor Growth Assay, and T-Cell Depletion

Dissociated organoids were resuspended in 100 μL of a 1:1 mixture of PBS and BME. Next, mice were anesthetized and the single-cell organoid suspension was injected into the flank. CD4/8 T-cell depletion was performed by treating mice with 100 μg anti-CD4 antibody (BioXCell, BXC-BE0003–1), anti-CD8 antibody (BioXCell, BXC-BE0061), or rat IgG2b isotype control (BioXCell, BXC-BE0086) twice per week via intraperitoneal injections. Treatment started 2 days after organoid injection.

Intrasplenic Injection

Dissociated tumor cells in PBS were slowly introduced into the spleen using a fine-gauge syringe. Access to the spleen was achieved through a small surgical incision in the left lateral abdomen, followed by gentle exteriorization of the spleen. Animals were euthanized 4 weeks after implantation of the modified tumor organoids.

Statistical Analysis

Statistical analysis of single-cell RNA sequencing data was performed using R (version 4.3.3) and the Seurat package (version 5.0.2), as outlined in the respective analysis sections. For comparisons of gene expression or gene set activity between cell groups (eg, split violin plots), the Wilcoxon rank-sum test was applied as implemented in Seurat. *P* values were adjusted for multiple comparisons using the Benjamini-Hochberg method unless otherwise specified. Additional statistical analyses were conducted in GraphPad Prism version 10 (GraphPad Software), unless stated otherwise. The statistical tests used, number of biological replicates, and sample sizes are provided in the corresponding figure legends. Data are presented as the mean ± standard error of the mean. Statistical significance is indicated as follows: $*P < .05$, $**P < .01$, $***P < .001$, and $****P < .0001$.

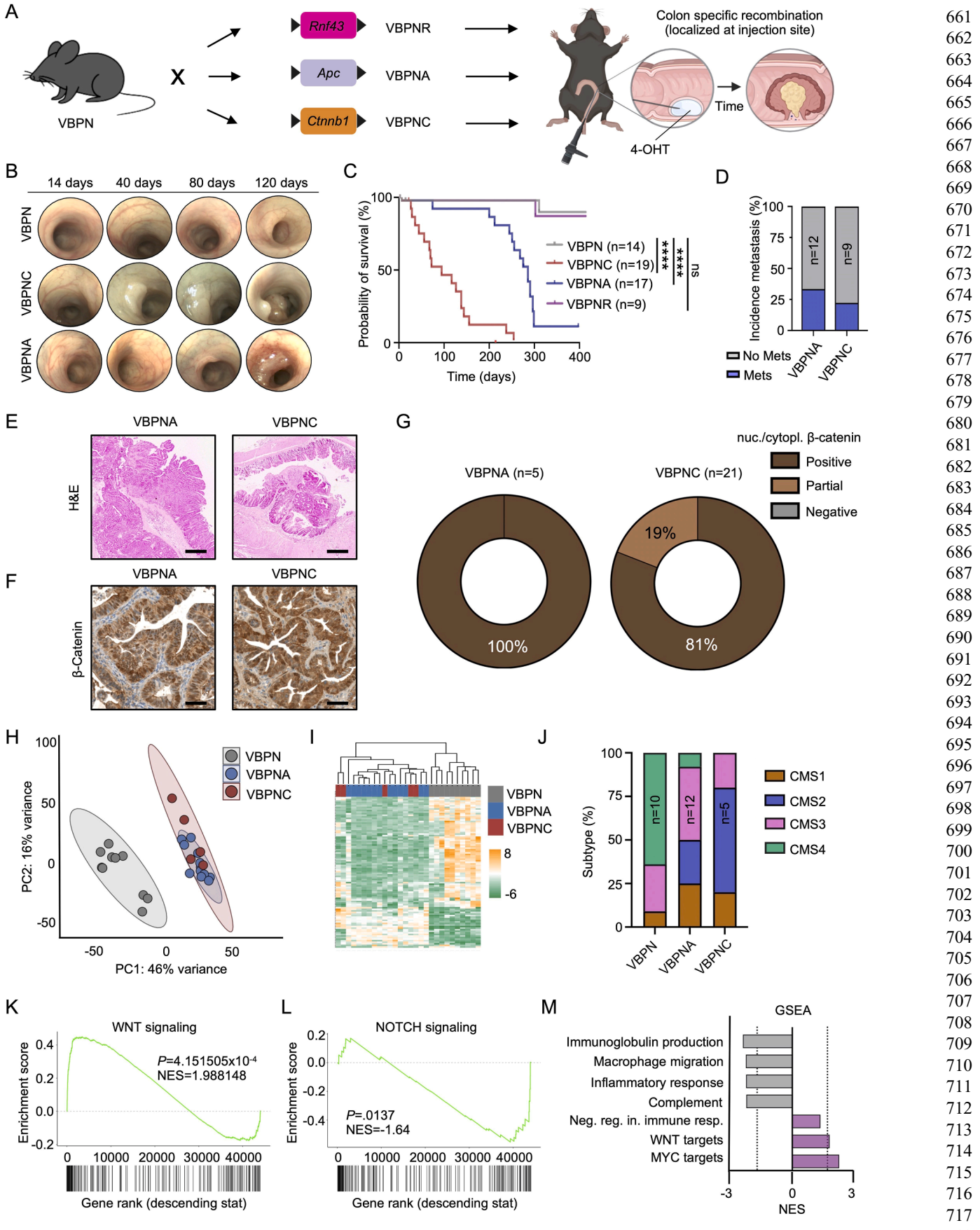
Results

Modeling Advanced Braf-Mutant Colorectal Cancer Uncovers WNT Activation

BRAF-mutant CRC has previously been associated with poor prognosis. Analysis of independent human cohorts confirmed the poor prognosis of *BRAF*-mutant CRC and identified distinct patterns of WNT pathway alterations in *BRAF*-mutant MSS and MSI tumors (Supplementary Figure 1A–C).[9,30] To model this aggressive CRC subtype, we intercrossed *Villin1*Cre^{ER} mice with a *Braf*^{V600E} and floxed *Trp53* allele (VBP) (Figure 1*A*), as there is a high frequency of *TP53* mutations observed in human MSS *BRAF*-mutant CRC.[31] Intraperitoneal injection of tamoxifen and subsequent recombination of floxed alleles in the intestine generated metastatic tumors (Figure 1*B–D*; Supplementary Figure 1*D*). We previously described that Notch1 activation is a driver of metastasis in *Kras*-mutant serrated CRC.[7] Therefore, we intercrossed a conditional Notch1 intracellular domain (N1icd) allele into VBP mice (VBPN, Figure 1*A*). The activation of Notch1 signaling upon Cre-recombination, significantly enhanced metastasis, whereas no impact on survival or number of tumors was detected (Figure 1*B* and *C*; Supplementary Figure 1*E*). To further characterize the molecular features of these tumors, we assessed WNT pathway activation by immunohistochemistry for β-catenin. In most VBPN tumors, WNT signaling was activated, as indicated by nuclear/cytoplasmic β-catenin localization and expression of the WNT target gene *Lgr5* (Figure 1*E* and *F*; Supplementary Figure 1*F* and *G*). To determine whether this WNT activation was associated with genetic alterations, we performed whole-exome sequencing of 10 VBPN tumors. Genetic alterations in the CRC driver gene *Ctnnb1* were detected in 40% of tumors, with mutations affecting the exon 3 residues S33, I35, and T41. Mutations at these sites are expected to impair β-catenin degradation and thereby promote β-catenin stabilization (Figure 1*G*). To assess the human relevance of our mouse model, we analyzed WNT signaling status in human *BRAF*-mutant MSS colorectal cancer. Approximately one-third of tumors showed nuclear/cytoplasmic β-catenin positivity and another subset

Figure 1. Genetic modeling of *Braf*-mutant colorectal cancer. (*A*) Schematic describing the genetics and induction of VBPN mice. (*B*) Kaplan-Meier curve of VBP (n = 19) and VBPN (n = 30) mice post induction. Log-rank (Mantel-Cox) test. (*C*) Bar graph showing the incidence of metastasis in VBP (n = 12) and VBPN (n = 18) mice. Statistical significance was assessed by Fisher's exact test. (*D*) Representative hematoxylin and eosin (H&E) image of VBPN carcinoma. Scale bar, 100 μm. (*E*) Proportion of tumors (VBPN) with nuclear/cytoplasmic β-catenin expression (n = 26). (*F*) Immunofluorescence of VBPN tumors. Scale bar, 50 μm. (*G*) Genetic alterations identified via whole-exome sequencing in tumors from VBPN mice (n = 10). The *upper panel* displays the full-length protein structure with mutations mapped to their amino acid positions. The *lower panel* provides an expanded schematic of exon 3, detailing the cluster of genomic alterations within this hotspot region. (*H*) Proportion of human *BRAF*-mutant MSS tumors with nuclear/cytoplasmic β-catenin expression (n = 10). (*I*) Immunofluorescence of human *BRAF*-mutant MSS tumors. Scale bar, 50 μm. (*J*) Oncoprint showing WNT pathway alterations and tumor mutational burden in human *BRAF*-mutant MSS CRCs (n = 270).

UNCORRECTED PROOF


A
VBPN
X
Rnf43
Apc
Ctnnb1
VBPNR
VBPNA
VBPNC
Colon specific recombination
(localized at injection site)
Time
4-OHT
B
14 days
40 days
80 days
120 days
VBPN
VBPNC
VBPNA
C
Probability of survival (%)
Time (days)
VBPN (n=14)
VBPNC (n=19)
VBPNA (n=17)
VBPNR (n=9)
****
****
ns
D
Incidence metastasis (%)
n=12
n=9
No Mets
Mets
VBPNA
VBPNC
E
VBPNA
VBPNC
H&E
F
VBPNA
VBPNC
β-Catenin
G
nuc./cytopl. β-catenin
Positive
Partial
Negative
VBPNA (n=5)
VBPNC (n=21)
100%
19%
81%
H
PC2: 16% variance
PC1: 46% variance
VBPN
VBPNA
VBPNC
I
VBPN
VBPNA
VBPNC
8
-6
J
Subtype (%)
n=10
n=12
n=5
CMS1
CMS2
CMS3
CMS4
VBPN
VBPNA
VBPNC
K
WNT signaling
Enrichment score
P=4.151505x10-4
NES=1.988148
Gene rank (descending stat)
L
NOTCH signaling
Enrichment score
P=.0137
NES=-1.64
Gene rank (descending stat)
M
GSEA
Immunoglobulin production
Macrophage migration
Inflammatory response
Complement
Neg. reg. in. immune resp.
WNT targets
MYC targets
NES

showed partial positivity, supporting conservation of this phenotype between VBPN tumors and human *BRAF*-mutant MSS CRC (Figure 1*H* and *I*; Supplementary Figure 1*H*). Histopathological analysis of lesions containing adjacent low-grade and high-grade dysplasia revealed that WNT activation, evidenced by nuclear/cytoplasmic β-catenin localization, was consistently observed in high-grade dysplastic regions, suggesting activation during tumor progression (Supplementary Figure 1*I*). Moreover, mutational profiling of 270 BRAF-mutant MSS CRC patients from 7 independent cohorts identified recurrent alterations in WNT pathway components, including *APC*, *RNF43*, *AXIN2*, and *CTNNB1* (Figure 1*J*). Comparison of *BRAF*-mutant MSS and MSI CRCs revealed distinct WNT alteration patterns. MSS tumors were dominated by constitutive, ligand-independent *APC* mutations, whereas MSI tumors showed a more heterogeneous landscape in which *RNF43* mutations, associated with ligand-dependent WNT activation, occurred at frequencies comparable to *APC* mutations (Supplementary Figure 1*J*). Together, these data demonstrate that the highly metastatic VBPN model recapitulates WNT pathway activation observed in human BRAF-mutant CRC.

WNT Activation Drives Malignant Transformation of Serrated Colorectal Cancer

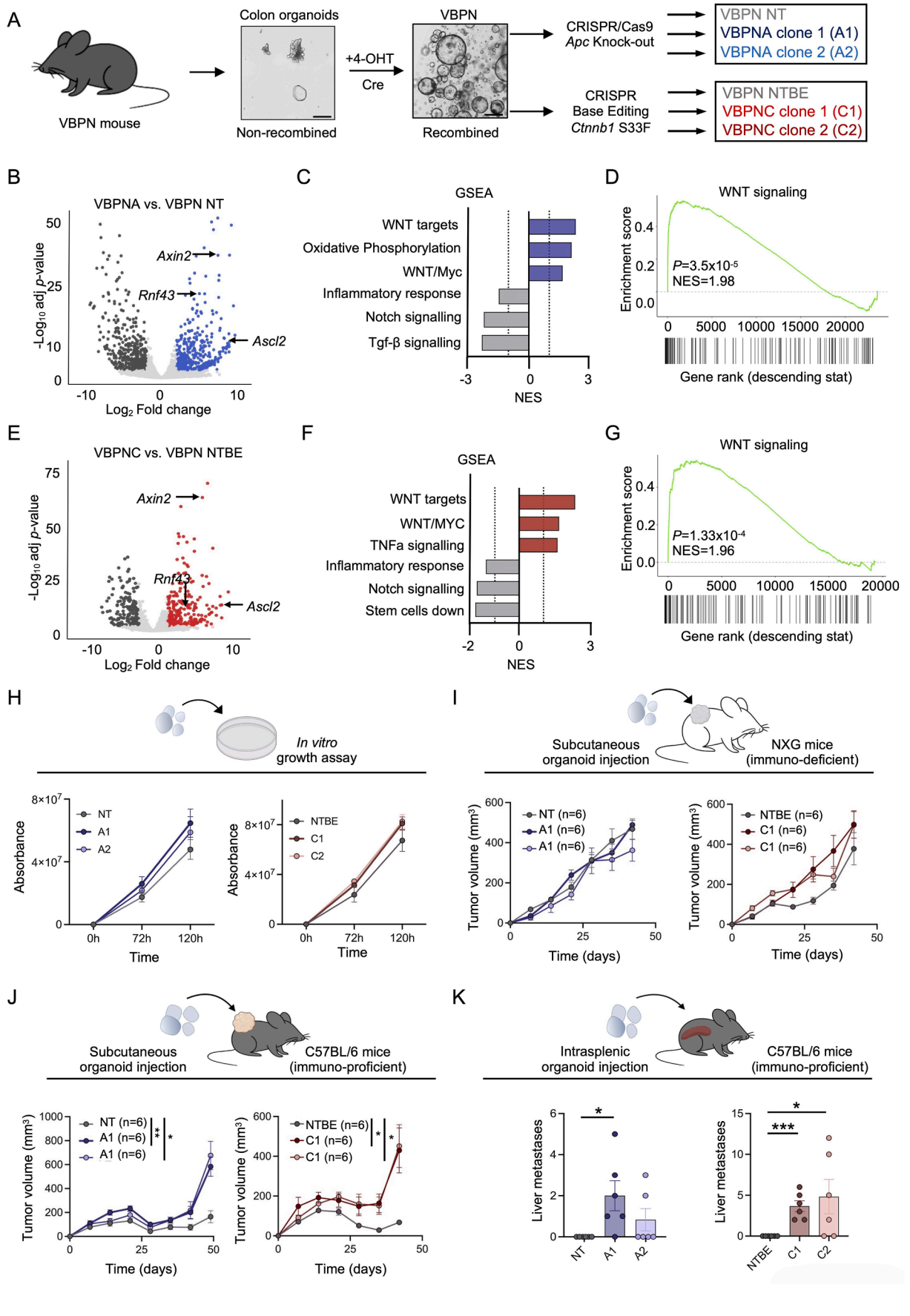
Next, we set out to define the functional role of genetic WNT pathway alterations in the progression of serrated CRC. To this end, we introduced driver mutations that were identified in the 270 human samples (Figure 1*J*). We intercrossed a floxed allele of *Rnf43*$^{fl/fl}$ (VBPNR), *Apc*$^{fl/+}$ (VBPNA) or an activating deletion of exon 3 in *Ctnnb1*$^{fl/+}$ (VBPNC). To determine whether this additional alteration leads to CRC development, we induced recombination at the proximal to mid colon by injection of 4-OHT. This induction generates a focal recombination at the site of injection and, different from the previously introduced model, leaves the remaining intestine unrecombined. Indeed, this induction resulted in tumor development only at the injection site, with no tumors observed elsewhere in the intestine (Figure 2*A* and *B*). This technology enabled us to specifically assess tumor initiation. Longitudinal monitoring showed that only VBPNC and VBPNA mice generated metastatic tumors, whereas VBPN or VBPNR did not within 1 year post injection (Figure 2*C* and *D*). Tumors arising in VBPNA and VBPNC showed strong nuclear/cytoplasmic localization of β-catenin (Figure 2*E*–*G*). RNA-sequencing data of VBPN tumors (intraperitoneal injection) or VBPNA/VBPNC tumors showed a clear separation of tumors, based on WNT activation status (Figure 2*H* and *I*). WNT activation resulted in a subtype switch from the mesenchymal CMS4 in VBPN to the WNT-high subtypes, CMS2 and CMS3, in VBPNA and VBPNC tumors (Figure 2*J*; Supplementary Figure 1*K*). This shift from the mesenchymal subtype to the WNT-high and metabolic subtypes[8] is in line with the activation of WNT signaling. Interestingly, activation of WNT signaling and the subtype switch co-occurred with a downregulation of Notch1-signaling activity (Figure 2*K* and *L*). Again, this agrees with our previous observation that Notch1 signaling is a major driver of CMS4.[7] Furthermore, we identified a strong downregulation of immune response signaling in WNT-high (VBPNA and VBPNC vs VBPN) tumors (Figure 2*M*). In sum, we provide functional evidence that WNT pathway activation is a central part of tumor initiation in *Braf*-mutant CRC.

WNT-Driven Immune Evasion In Vivo

Next, we investigated the effect of WNT activation on immune surveillance. To avoid acquisition of additional driver mutations in vivo and potential effects of tumor location, we isolated normal colonic epithelial cells from uninduced VBPN mice and established organoids, which were recombined ex vivo with 4-OHT (Figure 3*A*; Supplementary Figure 2*A*). The resulting spherical organoids grew independently of epidermal growth factor and were edited to generate isogenic *Rnf43*- or *Apc*-knockout lines or a *Ctnnb1* S33F mutation using CRISPR/Cas9 or base editing, respectively[32,33] (Figure 3*A*; Supplementary Figure 2*A*–*D*). Two independent clones per single guide RNA were analyzed to account for clonal effects. RNA sequencing revealed upregulation of canonical WNT targets and suppression of immune-regulatory processes in *Apc*- and *Ctnnb1*-mutant organoids (Figure 3*B*–*G*). Complementary quantitative polymerase chain reaction showed increased *Lgr5* expression in *Apc*- and *Ctnnb1*-mutant organoids, whereas *Rnf43* loss alone did not activate WNT target expression but retained responsiveness to WNT3a (Supplementary Figure 2*E* and *F*). Principal component analysis and gene set enrichment analysis further characterized the distinct transcriptional state of *Rnf43*-mutant organoids (Supplementary Figure 2*G* and *H*). TOP-GFP reporter organoids independently confirmed canonical WNT

Figure 2. WNT pathway alterations and tumor initiation in *Braf*-mutant models. (*A*) Breeding and induction strategy of VBPN, VBPNR, VBPNA, and VBPNC mice. (*B*) Colonoscopy pictures of indicated genotypes over time. (*C*) Kaplan-Meier curve of indicated genotypes post induction as outlined in (*A*). Statistical analysis was conducted with the log-rank (Mantel-Cox) test. (*D*) Incidence of metastasis in VBPNA (n = 12) and VBPNC (n = 9) mice. (*E*) Representative hematoxylin and eosin (H&E) image of VBPNA and VBPNC tumors. Scale bar, 400 μm. (*F*) Representative β-catenin stain of VBPNA and VBPNC tumors. Scale bar, 200 μm. (*G*) Percentage of tumors with nuclear/cytoplasmic β-catenin expression (n = 5 VBPNA; n = 21 VBPNC). (*H*) Principal component analysis plot of bulk RNA-sequencing data across genotypes (n = 10 VBPN; n = 12 VBPNA; n = 5 VBPNC). (*I*) Differentially expressed genes across genotypes. (*J*) CMS analysis across the genotypes. (*K*) Gene set enrichment analysis (GSEA) of VBPN vs VBPNA/VBPNC for WNT pathway activation. (*L*) GSEA of VBPN vs VBPNA/VBPNC for NOTCH-pathway activation. (*M*) GSEA of VBPN vs VBPNA/VBPNC for indicated gene sets. Adjusted *P* values shown in the enrichment plots in (*K*), (*L*), and (*M*) by applying the Benjamini-Hochberg procedure to control the false discovery rate across all tested gene sets.

UNCORRECTED PROOF



print & web 4C/FPO

activation in *Apc*- and *Ctnnb1*-mutant, but not *Rnf43*-mutant, lines (Supplementary Figure 2*I* and *J*).

To phenotypically characterize VBPNA and VBPNC organoids, we analyzed their proliferation in vitro. WNT activation did not alter organoid growth in vitro (Figure 3*H*). Screening of 140 compounds, most of which were clinically approved, revealed genotype-specific responses. VBPNR organoids, included because *RNF43* mutations predict responses to combined BRAF/EGFR inhibition,[24] showed greater sensitivity to targeted therapies, whereas *Apc*- and *Ctnnb1*-mutant organoids were resistant to BRAF and MEK inhibitors (Supplementary Figure 3*A*–*E*).

Next, we wanted to follow our observation of immune regulation by WNT signaling activity. To this end, we transplanted organoids into immunodeficient mice, which revealed no differences in tumor growth depending on WNT pathway alterations (Figure 3*I*). However, when transplanted into immuno-proficient C57BL/6 mice, both clones from VBPNA and VBPNC organoids showed significantly increased growth compared with the non-targeting controls (Figure 3*J*). This phenotype was also observed in a liver colonization assay, with metastases detected only in mice injected with *Apc*- or *Ctnnb1*-mutant VBPN organoids (Figure 3*K*). Whole-exome sequencing analysis of VBPN tumors showed no mutations in canonical regulators of antigen presentation, chemokine signaling, and immune modulation (*B2m*, *Tap1/2*, *Nlrc5*, *Jak1/2*, *Ccl5*, *Cxcl9/10*, and *Cd274*), suggesting that the downregulation of immune processes was not driven by other genetic events. These findings suggest that the enhanced WNT activation leads to immune suppression, enhancing tumor growth and metastasis.

WNT Activation Rewires the Tumor Immune Microenvironment

To define how WNT activation remodels the tumor microenvironment, we performed CITE-seq on 11,559 cells from VBPN, VBPNA, and VBPNC tumors (Figure 4*A*–*C*). Five cancer-cell clusters were identified, with expansion of cluster 3 and reduction of cluster 2 in WNT-activated tumors. Cluster 3 showed increased *Axin2* and *Lgr5* expression, and cancer cells from VBPNA and VBPNC tumors were enriched for WNT signatures (Figure 4*D*). WNT activation also shifted neutrophils and macrophages toward myeloid-derived suppressor cell- and M2-like states (Supplementary Figure 4*A*–*D*) and altered T-cell composition, increasing $TCF7^+$ progenitor-like $CD4^+$ T cells and exhausted $CD8^+$ T cells, the latter of which were absent from control tumors (Figure 4*E*–*G*; Supplementary Figure 4*E*).

To assess the functional contribution of these T-cell populations, we depleted $CD4^+$ or $CD8^+$ T cells following transplantation of VBPNA organoids into C57BL/6 mice (Figure 4*H*; Supplementary Figure 5*A* and *B*). $CD4^+$ T-cell depletion accelerated tumor growth, whereas $CD8^+$ T-cell depletion reduced it (Figure 4*I* and *J*), revealing opposing roles of these T-cell subsets. Single-cell analysis following depletion further showed opposing remodeling of myeloid populations, antigen presentation, and interferon signaling after $CD4^+$ vs $CD8^+$ T-cell depletion (Figure 4*K*–*N*; Supplementary Figure 5*C*–*J*). Together, these findings indicate that WNT-high *BRAF*-mutant CRCs establish an immune state that limits effective tumor recognition.

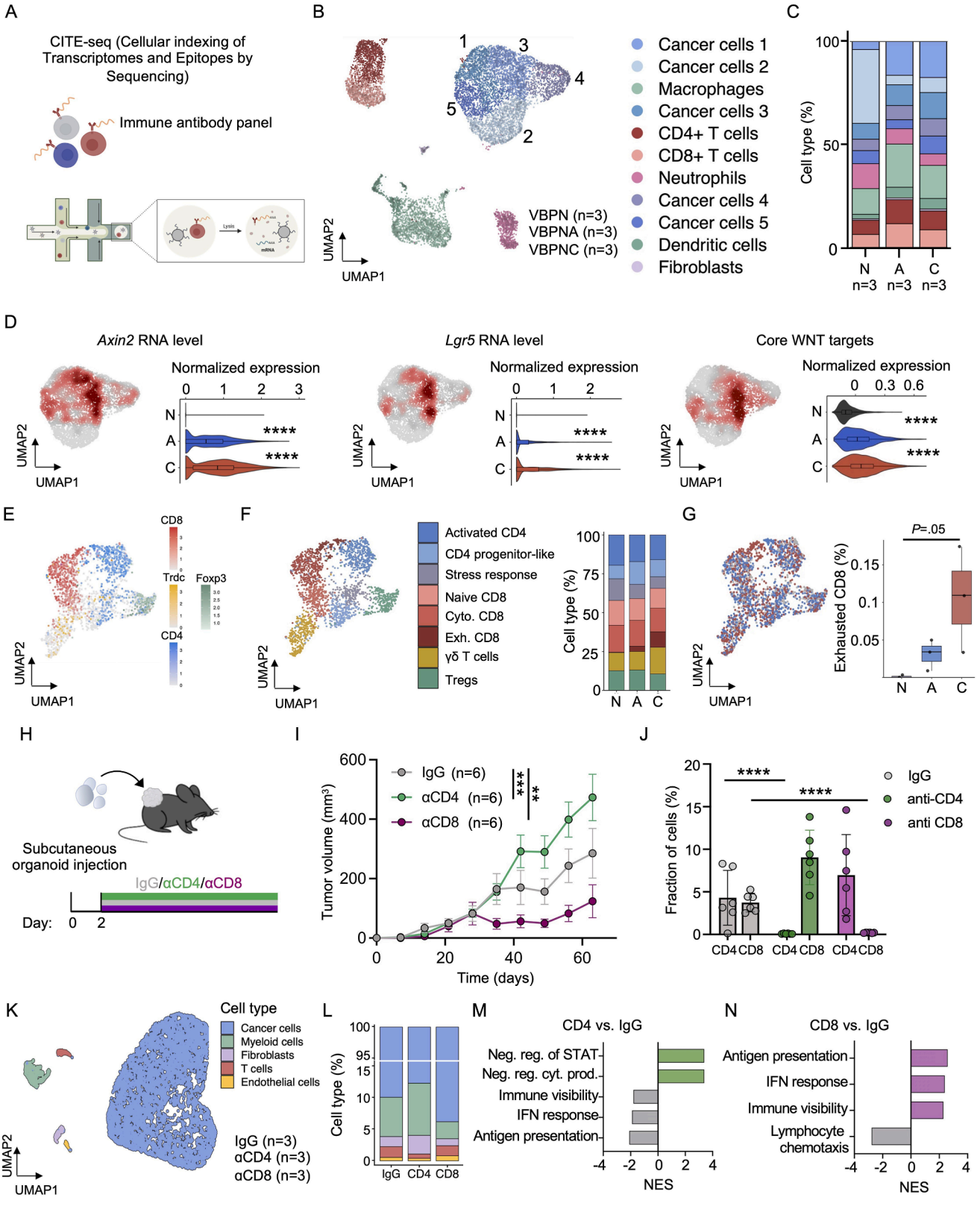
Downregulation of C-C motif chemokine ligand 20 by WNT Signaling Promotes Tumor Progression

To identify mediators linking WNT activation to altered T-cell states, we analyzed differentially expressed genes in VBPNA and VBPNC organoids and identified *Ccl20* as consistently downregulated (Figure 5*A*–*C*). C-C motif chemokine ligand 20 (CCL20) recruits $CD4^+$ T cells through C-C chemokine receptor type 6 (CCR6).[34] Notably, reduced *Ccl20* expression was accompanied by increased *Axin2* expression, confirming enhanced WNT pathway activity (Figure 5*B* and *C*). Consistently, treatment of VBPN organoids with Wnt-Fc, a potent recombinant ligand designed to induce WNT signaling, led to *Ccl20* downregulation, which negatively correlated with *Axin2* expression (Figure 5*D*). We further validated this relationship in the human MSS *BRAF*-mutant HT29 cell line, by treating with a Glycogen Synthase Kinase-3 inhibitor (CHIR-99021), which induced *AXIN2* expression and concomitantly led to a decrease in *CCL20* levels (Figure 5*E*), confirming WNT-dependent regulation of CCL20 in murine and human cells.

To assess the functional relevance of CCL20 suppression in vivo, we generated VBPNC organoids ectopically expressing *Ccl20*, along with an empty vector control (Figure 5*F*). Validation confirmed robust *Ccl20* expression (Figure 5*G*), thus we performed injections into immunocompetent C57BL/6 mice alongside empty vector controls. Strikingly, *Ccl20*-overexpressing cells showed significantly reduced tumor growth compared with controls (Figure 5*H*). Endpoint tumor weights were also significantly decreased in the *Ccl20*-overexpressing tumors (Figure 5*I*). Together, these findings demonstrate that WNT pathway activation suppresses CCL20 expression, thereby promoting tumor growth.

Figure 3. Immune evasion by WNT activation. (*A*) Schematic describing the generation of isogenic VBPNA and VBPNC organoids. Scale bar, 250 μm. (*B*) Volcano plot of differentially expressed genes from VBPN vs VBPNA organoids. (*C*) Gene set enrichment analysis (GSEA) of VBPN vs VBPNA organoids for indicated gene sets. (*D*) GSEA of VBPN vs VBPNA organoids for WNT pathway activation. (*E*) Volcano plot of differentially expressed genes from VBPN vs VBPNC organoids. (*F*) GSEA of VBPN vs VBPNC organoids for indicated gene sets. (*G*) GSEA of VBPN vs VBPNC organoids for WNT pathway activation. (*H*) Growth assay of indicated organoids in vitro (n = 2). (*I*) Tumor growth of subcutaneous tumors in immunodeficient mice (n = 6 per group). (*J*) Tumor growth of subcutaneous tumors in immuno-proficient mice (n = 6 per group). (*K*) Number of liver metastases in immuno-proficient mice. Data were analyzed using an unpaired *t* test (n = 6). Data in (*H*), (*I*), and (*J*) were analyzed by 2-way analysis of variance. Adjusted *P* values shown in the enrichment plots in (*D*) and (*G*) by applying the Benjamini-Hochberg procedure to control the false discovery rate across all tested gene sets.

UNCORRECTED PROOF



print & web 4C/FPO

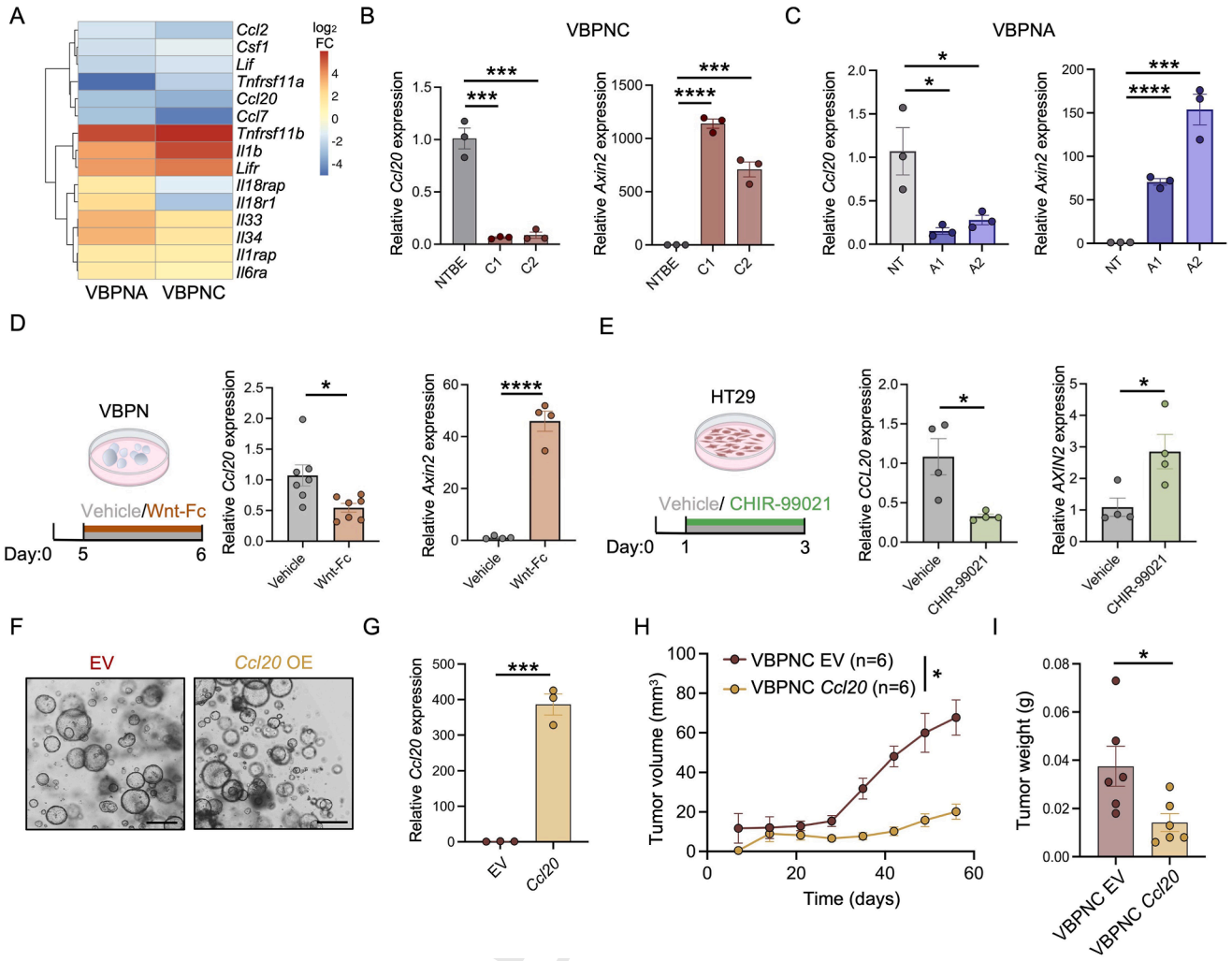


Figure 5. WNT/CCL20/CCR6 axis in CRC. (*A*) Top 20 differentially expressed cytokine and chemokine genes across VBPNA and VBPNC organoids compared with VBPN. (*B* and *C*) Relative *Ccl20* and *Axin2* mRNA expression in VBPNC (*B*) and VBPNA (*C*) organoids (n = 3). (*D*) Relative *Ccl20* (n = 7) and *Axin2* (n = 5) messenger RNA (mRNA) expression in VBPN organoids following 24 hours of treatment with Wnt-Fc. (*E*) Relative *CCL20* and *AXIN2* mRNA expression in HT29 cells following 48 hours of treatment with CHIR-99021 (n = 4). (*F*) VBPNC organoids with empty vector (EV) and *Ccl20* overexpression (OE) organoid lines. Scale bar, 250 μm. (*G*) Relative *Ccl20* mRNA expression following OE in VBPNC (n = 3). (*H*) Tumor growth of subcutaneous tumors (n = 6). Data were analyzed by 2-way analysis of variance. (*I*) Tumor weight at endpoint of subcutaneous VBPNC EV and VBPNC *Ccl20* tumors (n = 6). Data in (*B*), (*C*), (*D*), (*E*), (*G*), and (*I*) were analyzed by unpaired *t* test.

Figure 4. Immune phenotyping of *Braf*-mutant tumors. (*A*) Schematic describing the CITE-seq workflow. (*B*) UMAP plot (11,559 cells) showing the cellular distribution of VBPN NT (n = 3), VBPNA (n = 3) and VBPNC (n = 3) tumors. (*C*) Bar plot describing the distribution of cell types across genotypes. N = nontargeting VBPN; A = VBPNA; C = VBPNC. (*D*) WNT target gene expression in the epithelial cell compartment of tumors. Statistical significance was assessed by Wilcoxon rank-sum test with Benjamini-Hochberg correction. N = nontargeting VBPN; A = VBPNA; C = VBPNC. (*E*) UMAP plot showing T-cell annotations. (*F*) Quantification of T-cell state across genotypes. N = nontargeting VBPN; A = VBPNA; C = VBPNC. (*G*) UMAP and box plot showing CD8 T-cell exhaustion cluster across genotypes. Data were analyzed by unpaired *t* test. N = nontargeting VBPN; A = VBPNA; C = VBPNC. (*H*) Experimental setup for T-cell depletion in vivo. (*I*) Tumor growth curve under T-cell depletion. Data were analyzed by 2-way analysis of variance (n = 6 per group). (*J*) Quantification of T-cell depletion at endpoint. Statistical analysis was conducted by a 2-way analysis of variance. (*K*) UMAP of 7995 cells from single-cell RNA sequencing of tumors from (*H*)–(*J*) treated with immunoglobulin (Ig)G (n = 3), CD4 (n = 3), CD8 (n = 3). (*L*) Proportion plot of different cell types in the tumors from different treatments. (*M*) Gene set enrichment analysis (GSEA) of cancer cells from CD4 depletion vs IgG. (*N*) GSEA of cancer cells from CD8 depletion versus IgG.

print & web 4C/FPO

UNCORRECTED

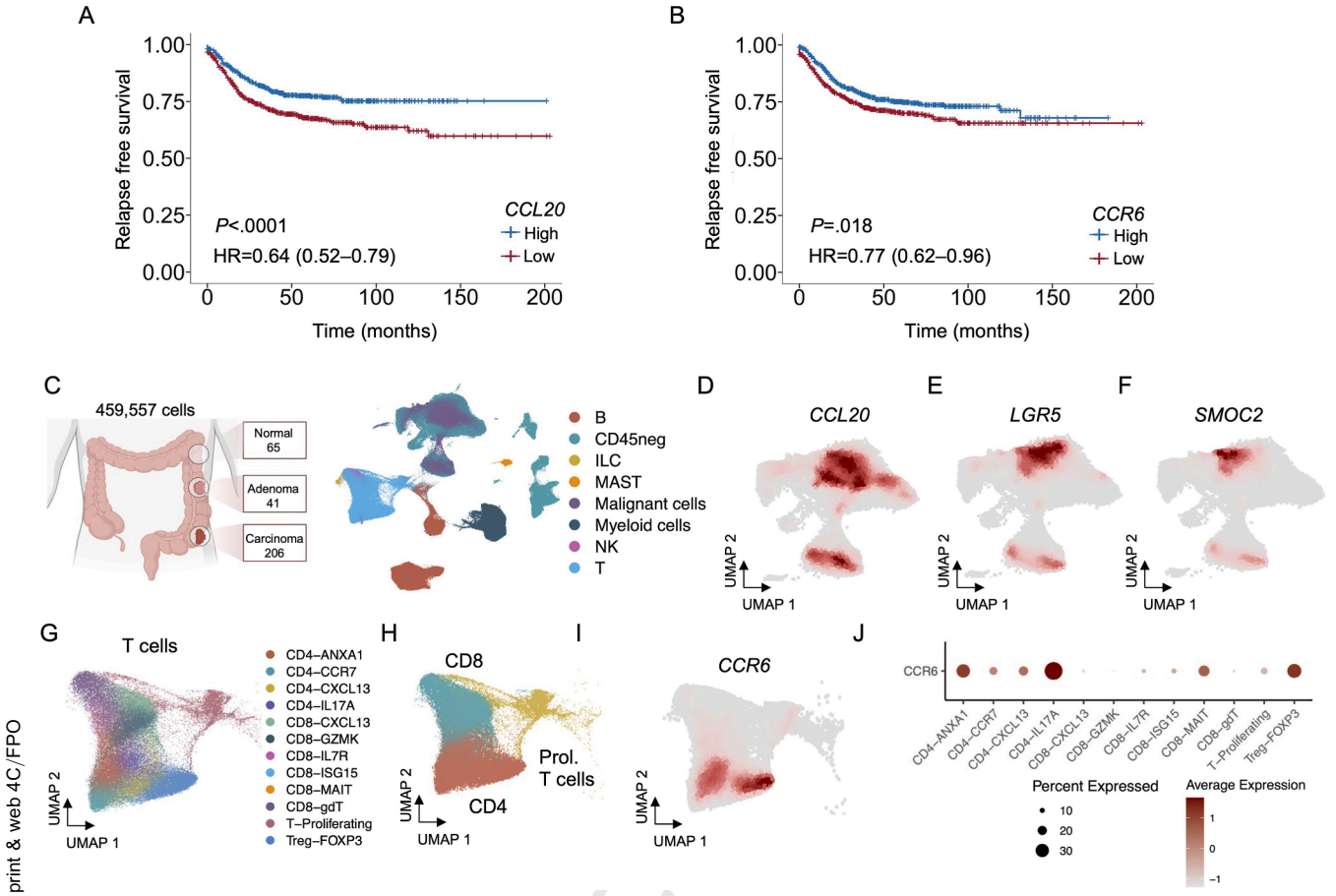


Figure 6. WNT/CCL20/CCR6 axis in human CRC. (*A* and *B*) Kaplan-Meier curves correlating relapse-free survival with median *CCL20* (*A*) and *CCR6* (*B*) expression (n = 1336). Data in (*A*) and (*B*) were analyzed using the log-rank test. (*C*) Single-cell atlas of human CRC adapted from Chu et al.[40] The analyzed subset comprised 312 samples and 459,557 cells. (*D*) UMAP density plot of *CCL20* expression in the malignant epithelial cell compartment. (*E*) *LGR5* expression in the malignant epithelial cell compartment. (*F*) *SMOC2* expression in the malignant epithelial cell compartment. (*G*) UMAP of the T-cell cluster of the data set with T-cell subtypes indicated. (*H*) T-cell cluster with CD8, CD4, or proliferating T cells indicated. (*I*) *CCR6* expression in the T-cell cluster. (*J*) Expression analysis of *CCR6* in the different T-cell clusters. (*K*) Proposed model of WNT-driven immune evasion in *Braf*-mutant CRC. Q11

CCL20-CCR6 Axis Is Conserved in Human Colorectal Cancer

To investigate the link between WNT pathway activation, *Ccl20* downregulation, and reduced $CD4^+$ T-cell recruitment in the human setting, we analyzed a cohort of 1,336 patients (Figure 6*A* and *B*). Tumors were stratified into CCR6-high vs CCR6-low and CCL20-high vs CCL20-low groups. Interestingly, lower expression of either factor was associated with poor prognosis.

Next, we investigated this axis in a large single-cell RNA-sequencing dataset from human samples (n = 312) (Figure 6*C*). After subsetting malignant epithelial cells, we identified a distinct CCL20-expressing subcluster (Figure 6*D*). This cluster showed different expression patterns compared with WNT target genes *LGR5* and *SMOC2* (Figure 6*E* and *F*), supporting an inverse association between WNT pathway activity and *CCL20* expression in human CRC cells. We then analyzed the T-cell compartment in the same dataset (Figure 6*G*) and detected *CCR6* expression exclusively within the $CD4^+$ T-cell population (Figure 6*H* and *I*). More detailed annotation revealed that CCR6 expression was enriched in CD4-ANXA1, CD4-IL17A, and Treg-FOXP3 subsets (Figure 6*J*), indicating that multiple $CD4^+$ T-cell states may respond to cancer cell–derived CCL20. Together, these findings indicate that the WNT-CCL20-CCR6 axis is conserved in human CRC and suggest that WNT-driven suppression of CCL20 may limit $CCR6^+$ $CD4^+$ T-cell recruitment, thereby contributing to impaired antitumor immunity and poorer outcomes.

Discussion

Here, we identify a mechanism of WNT signaling-driven transformation of SSA to serrated CRC, characterized by nuclear/cytoplasmic accumulation of β-catenin during the transition from low-grade to high-grade dysplasia. Modeling human-relevant genetic alterations, recurrently detected in *BRAF*-mutant serrated CRC, revealed a critical

print & web 4C/FPO
UNCORRECTED

role for Notch1 signaling in driving tumor progression and metastasis to clinically relevant sites such as the liver and lungs. Similar to human serrated CRC, these mouse models show WNT pathway activation in the course of malignant transformation. WNT pathway activation was essential for progression by driving immunosuppression.

Our data show that, similar to *Kras*-mutant serrated CRC,[7] *Notch1* activation promotes metastatic progression in *Braf*-mutant models. Functional interrogation of recurrent WNT pathway alterations demonstrated that *Apc* and *Ctnnb1* mutations robustly promoted tumor initiation, whereas *Rnf43* loss was insufficient. This distinction was mirrored in human cohorts, in which *RNF43* alterations were more prominent in *BRAF*-mutant MSI tumors, whereas *APC* alterations predominated in MSS tumors. The association of *Apc*- and *Ctnnb1*-mutant tumors with CMS2/3 further suggests that the consequences of WNT activation depend on pathway strength and tumor context. Although *APC* alterations have been associated with poor prognosis in *BRAF*-mutant CRC,[35] strong WNT activation may establish a molecular state distinct from the WNT-low, CMS4-like phenotype of VBPN tumors. Serrated CRC also can progress without substantial WNT activation,[1] indicating that WNT-low tumors may evade immune surveillance through alternative mechanisms, including a transforming growth factor β–high immunosuppressive tumor microenvironment, as previously described.[7] Thus, individual WNT pathway alterations are not functionally equivalent but differentially shape tumor initiation, molecular subtype, and immune regulation. Collectively, our findings provide functional evidence that WNT pathway activation during the transition to high-grade dysplasia is a key driver of malignant progression in *BRAF*-mutant serrated CRC.

The observation that WNT activation in *BRAF*-mutant CRC suppresses inflammatory and immune-regulatory responses is consistent with previous correlative studies linking WNT pathway activation in CRC to immune exclusion.[36,37] The unexpected reduction in tumor growth following $CD8^+$ T-cell depletion contrasted with the accelerated growth following $CD4^+$ T-cell depletion, suggesting opposing functions of these T-cell subsets and may reflect a predominance of functionally exhausted $CD8^+$ T cells within these tumors. Rather than mediating effective cytotoxicity, such cells may contribute to adaptive immune resistance through sustained inflammatory signaling and immunoediting. In line with this, the inverse regulation of antigen presentation machinery and interferon (IFN) signaling following $CD4^+$ vs $CD8^+$ T-cell depletion suggests that $CD4^+$ T cells are required to maintain IFN-driven antigen presentation, whereas $CD8^+$ T cells may impose selective pressure that favors antigen-presenting machinery-low tumor variants or induces feedback inhibition of IFN responsiveness. Further functional characterization, including cytokine profiling, exhaustion marker analysis, assessment of suppressive pathways, and ex vivo co-culture assays, will be necessary to disentangle whether these effects are driven by direct suppressive functions of specific T-cell subsets or arise indirectly through their impact on the broader tumor microenvironment.

WNT-driven immune evasion has also been reported in melanoma and hepatocellular carcinoma, where WNT activation impairs $CD8^+$ T-cell priming by suppressing dendritic-cell recruitment through reduced CCL4 and CCL5 expression.[38,39] Our findings reveal a related but distinct mechanism in CRC, in which WNT activation suppresses CCL20 expression. The reduced tumor growth following ectopic *Ccl20* expression supports the functional relevance of this chemokine axis. Together, these findings suggest that chemokine suppression represents a conserved mechanism of WNT-driven immune evasion, while the affected chemokine and immune-cell populations are tumor-context dependent. Our data therefore support investigating WNT pathway inhibition as a strategy to promote immune reprogramming and sensitize MSS CRC to immune checkpoint blockade.

Overall, we show that complex genetic interactions are not merely additive but synergistic, essentially rewiring transcriptional programs. Consequently, altering the tumor microenvironment is critical for tumor-cell–mediated immune evasion. Understanding this crosstalk and what individual mutations contribute to the cancer cell state and tumor microenvironment are essential for designing rational combination therapies and stratifying patients by functional oncogenic programs rather than single-gene alterations.

Supplementary Material

Note: To access the supplementary material accompanying this article, visit the online version of *Gastroenterology* at www.gastrojournal.org, and at http://doi.org/10.1053/j.gastro.2026.07.035.

References

1. Aiderus A, Barker N, Tergaonkar V. Serrated colorectal cancer: preclinical models and molecular pathways. Trends Cancer 2024;10:76–91.
2. Fearon ER, Vogelstein B. A genetic model for colorectal tumorigenesis. Cell 1990;61:759–767.
3. Nakanishi Y, Diaz-Meco MT, Moscat J. Serrated Colorectal cancer: the road less travelled? Trends Cancer 2019;5:742–754.
4. JE IJ, Vermeulen L, Meijer GA, et al. Serrated neoplasia-role in colorectal carcinogenesis and clinical implications. Nat Rev Gastroenterol Hepatol 2015;12:401–409.
5. Fennell L, Kane A, Liu C, et al. Braf mutation induces rapid neoplastic transformation in the aged and aberrantly methylated intestinal epithelium. Gut 2022;71:1127–1140.
6. Rad R, Cadinanos J, Rad L, et al. A genetic progression model of Braf(V600E)-induced intestinal tumorigenesis reveals targets for therapeutic intervention. Cancer Cell 2013;24:15–29.
7. Jackstadt R, van Hooff SR, Leach JD, et al. Epithelial NOTCH signaling rewires the tumor microenvironment of colorectal cancer to drive poor-prognosis subtypes and metastasis. Cancer Cell 2019;36:319–336.e7.

UNCORRECTED PROOF

ARTICLE IN PRESS

8. Guinney J, Dienstmann R, Wang X, et al. The consensus molecular subtypes of colorectal cancer. Nat Med 2015; 21:1350–1356.
9. Yaeger R, Chatila WK, Lipsyc MD, et al. Clinical sequencing defines the genomic landscape of metastatic colorectal cancer. Cancer Cell 2018;33:125–136.e3.
10. Wu JM, Montgomery EA, Iacobuzio-Donahue CA. Frequent beta-catenin nuclear labeling in sessile serrated polyps of the colorectum with neoplastic potential. Am J Clin Pathol 2008;129:416–423.
11. Yachida S, Mudali S, Martin SA, et al. Beta-catenin nuclear labeling is a common feature of sessile serrated adenomas and correlates with early neoplastic progression after BRAF activation. Am J Surg Pathol 2009; 33:1823–1832.
12. Weisenberger DJ, Siegmund KD, Campan M, et al. CpG island methylator phenotype underlies sporadic microsatellite instability and is tightly associated with BRAF mutation in colorectal cancer. Nat Genet 2006; 38:787–793.
13. Blaker H, Alwers E, Arnold A, et al. The association between mutations in BRAF and colorectal cancer-specific survival depends on microsatellite status and tumor stage. Clin Gastroenterol Hepatol 2019;17:455–462.e6.
14. Cornish AJ, Gruber AJ, Kinnersley B, et al. The genomic landscape of 2,023 colorectal cancers. Nature 2024; 633:127–136.
15. De Sousa EMF, Wang X, Jansen M, et al. Poor-prognosis colon cancer is defined by a molecularly distinct subtype and develops from serrated precursor lesions. Nat Med 2013;19:614–618.
16. Langner C. Serrated and non-serrated precursor lesions of colorectal cancer. Dig Dis 2015;33:28–37.
17. Lannagan TR, Jackstadt R, Leedham SJ, et al. Advances in colon cancer research: in vitro and animal models. Curr Opin Genet Dev 2021;66:50–56.
18. Bond CE, Liu C, Kawamata F, et al. Oncogenic BRAF mutation induces DNA methylation changes in a murine model for human serrated colorectal neoplasia. Epigenetics 2018;13:40–48.
19. Tauriello DVF, Batlle E. Targeting the microenvironment in advanced colorectal cancer. Trends Cancer 2016; 2:495–504.
20. Wellenstein MD, de Visser KE. Cancer-cell-intrinsic mechanisms shaping the tumor immune landscape. Immunity 2018;48:399–416.
21. Lakatos E, Gunasri V, Zapata L, et al. Epigenetically driven and early immune evasion in colorectal cancer evolution. Nat Genet 2025;57:3039–3049.
22. Loree JM, Kopetz S. Recent developments in the treatment of metastatic colorectal cancer. Ther Adv Med Oncol 2017;9:551–564.
23. Kopetz S, Grothey A, Tabernero J. Encorafenib, binimetinib, and cetuximab in BRAF V600E-mutated colorectal cancer. Reply. N Engl J Med 2020;382:877–878.
24. Elez E, Ros J, Fernandez J, et al. RNF43 mutations predict response to anti-BRAF/EGFR combinatory therapies in BRAF(V600E) metastatic colorectal cancer. Nat Med 2022;28:2162–2170.
25. Ruiz-Saenz A, Atreya CE, Wang C, et al. A reversible SRC-relayed COX2 inflammatory program drives resistance to BRAF and EGFR inhibition in BRAF(V600E) colorectal tumors. Nat Cancer 2023;4:240–256.
26. Tian J, Chen JH, Chao SX, et al. Combined PD-1, BRAF and MEK inhibition in BRAF(V600E) colorectal cancer: a phase 2 trial. Nat Med 2023;29:458–466.
27. Morris VK, Parseghian CM, Bahrambeigi V, et al. Phase 1/2 trial of encorafenib, cetuximab, and nivolumab in microsatellite stable BRAF(V600E) metastatic colorectal cancer. Cancer Cell 2025;43:2106–2118.e3.
28. Sánchez-Rivera FJ, Diaz BJ, Kastenhuber ER, et al. Base editing sensor libraries for high-throughput engineering and functional analysis of cancer-associated single nucleotide variants. Nat Biotechnol 2022; 40:862–873.
29. Vaquero-Siguero N, Schleussner N, Volk J, et al. Modeling colorectal cancer progression reveals niche-dependent clonal selection. Cancers (Basel) 2022; 14:4260.
30. Hoadley KA, Yau C, Hinoue T, et al. Cell-of-origin patterns dominate the molecular classification of 10,000 tumors from 33 types of cancer. Cell 2018;173:291–304.e6.
31. Bond CE, Umapathy A, Ramsnes I, et al. p53 mutation is common in microsatellite stable, BRAF mutant colorectal cancers. Int J Cancer 2012;130:1567–1576.
32. Roper J, Tammela T, Cetinbas NM, et al. Corrigendum: In vivo genome editing and organoid transplantation models of colorectal cancer and metastasis. Nat Biotechnol 2017;35:1211.
33. Katti A, Foronda M, Zimmerman J, et al. GO: a functional reporter system to identify and enrich base editing activity. Nucleic Acids Res 2020;48:2841–2852.
34. Liao F, Rabin RL, Smith CS, et al. CC-chemokine receptor 6 is expressed on diverse memory subsets of T cells and determines responsiveness to macrophage inflammatory protein 3 alpha. J Immunol 1999; 162:186–194.
35. Fennell LJ, Kane A, Liu C, et al. APC mutation marks an aggressive subtype of BRAF mutant colorectal cancers. Cancers (Basel) 2020;12:1171.
36. Grasso CS, Giannakis M, Wells DK, et al. Genetic mechanisms of immune evasion in colorectal cancer. Cancer Discov 2018;8:730–749.
37. Luke JJ, Bao R, Sweis RF, et al. WNT/beta-catenin pathway activation correlates with immune exclusion across human cancers. Clin Cancer Res 2019; 25:3074–3083.
38. Ruiz de Galarreta M, Bresnahan E, Molina-Sanchez P, et al. beta-Catenin activation promotes immune escape and resistance to anti-PD-1 therapy in hepatocellular carcinoma. Cancer Discov 2019;9:1124–1141.
39. Spranger S, Bao R, Gajewski TF. Melanoma-intrinsic beta-catenin signalling prevents anti-tumour immunity. Nature 2015;523:231–235.
40. Chu X, Li X, Zhang Y, et al. Integrative single-cell analysis of human colorectal cancer reveals patient stratification with distinct immune evasion mechanisms. Nat Cancer 2024;5:1409–1426.

UNCORRECTED PROOF

ARTICLE IN PRESS

Received January 16, 2026. Accepted July 28, 2026.

Correspondence
Address correspondence to: Rene Jackstadt, PhD, German Cancer Research Center, Cancer Progression and Metastasis Group, Im Neuenheimer Feld 280, 69120 Heidelberg, Germany. e-mail: r.jackstadt@dkfz.de.

Acknowledgments
The authors are grateful for technical support from Gabriele Schmidt and Raja Flüchter. We acknowledge the DKFZ - scOpenLab, Sequencing OpenLab, Genomics Core Facility, flow cytometry facility, Preclinical and Translational Pathology, and Central Animal facilities (ZPF) for excellent service. Schematics were created with BioRender.

CRediT Authorship Contributions
Manuel Mastel, PhD (Conceptualization: Lead; Writing – review & editing: Lead)
Aitana Guiseris Martinez, MSc (Visualization: Equal; Writing – review & editing: Lead)
Umberto Pozza, MSc (Methodology: Supporting)
Jasmin Meier, MSc (Methodology: Equal)
Ioannis Chiotakakos, MSc (Methodology: Supporting)
Sandra Jaun, Technician (Methodology: Supporting)
Carolin Artmann, BSc (Methodology: Supporting)
Gabriele Diamante, MSc (Methodology: Supporting)
Georgakopoulos Nikolaos, MSc (Methodology: Supporting)
Philipp Albrecht, MSc (Methodology: Supporting), Yvonne Petersen, Tech (Methodology: Supporting)
Saskia Reuter, MSc (Methodology: Supporting)
Barbara Schmitt, Tech (Methodology: Supporting)
Michael Günther, PhD (Methodology: Supporting)
Istiffa Nurfauziah, MSc (Methodology: Supporting)
Ian Ghezzi, PhD (Methodology: Supporting)
Kyanna Ouyang, M.Sc. (Methodology: Supporting)
Michael D. Milsom, PhD (Methodology: Supporting)
Alexandra Thiran, Dr (Methodology: Equal)
Jens Puschhof, PhD (Methodology: Supporting)
Nic Reitsam, PhD (Methodology: Supporting)
Kim Boonekamp, PhD (Methodology: Supporting)
Johannes Betge, PhD (Methodology: Supporting)
Steffen Ormanns, PhD (Conceptualization: Supporting)
Michael Boutros, PhD (Resources: Equal)
Rene Jackstadt, PhD (Conceptualization: Lead; Project administration: Lead; Supervision: Lead; Writing – original draft: Lead; Writing – review & editing: Equal)

Conflicts of interest
This author discloses the following: Nic G. Reitsam received travel compensation from Bruker Spatial Biology, which was not related to this work. The remaining authors disclose no conflicts.

Funding
Rene Jackstadt was supported by the Dietmar Hopp Foundation, the Dr. Rolf M. Schwiete Foundation (2021–032), the Wilhelm Sander Foundation (2022.049.1), the German Federal Ministry of Education and Research (BMBF; 01KD2206Q/SATURN3), and the Deutsche Forschungsgemeinschaft (JA 2558/3–1, JA 2558/4–1, JA 2558/6–1, JA 2558/8–1 and JA 2558/9–1 [FOR 5806]). Nic G. Reitsam is supported by the clinician scientist program of the Faculty of Medicine, University of Augsburg, Augsburg, Germany. Research in the Group of Johannes Betge was supported by the Hector Foundation II and by the Deutsche Forschungsgemeinschaft (FOR 5806). Research in the group of Michael Boutros was supported by Deutsche Forschungsgemeinschaft (CRC 1324 and FOR 5806). Fellowships were provided by the Helmholtz International PhD Graduate School to Manuel Mastel and Gabriele Diamante, The Cancer-TRAX program to Ioannis Chiotakakos, the DKFZ-MOST program to Nikolaos Georgakopoulos, and by the Mercksche Society for Art and Science to Aitana Guiseris Martinez. Manuel Mastel received a Joachim Herz foundation fellowship.

Data Availability
All raw data and processed data objects are available through ArrayExpress and the European Nucleotide Archive (ENA) under the accession numbers E-MTAB-17076 (RNA-seq of tumors), E-MTAB-17082 (RNA-seq of organoids), E-MTAB-17099 (CITE-seq), E-MTAB-17103 (exon sequencing), and E-MTAB-17106 (scRNA-seq). No new software has been developed for the analysis of the datasets. Example code for figure generation starting from data on ArrayExpress is available on GitHub (https://github.com/ManuelMastel/BRAF-mutant-colorectal-cancer).

UNCORRECTED PROOF